

## Elucidating morphological effects in membrane mineral fouling using real-time particle imaging and impedance spectroscopy

Chidiebere S. Nnebuo, Denise Hambsch, Oded Nir\*✉

*Department of Desalination and Water Treatment, Zuckerberg Institute for Water Research,  
Jacob Blaustein Institutes for Desert Research, Ben-Gurion University of the Negev, Sede-Boqer  
Campus 84990, Israel*

\*Corresponding author ✉ [odni@bgu.ac.il](mailto:odni@bgu.ac.il)

### Supporting information

#### 1.0 Membrane polyelectrolyte layer-by-layer (LBL) coating:

Static layer by layer coating procedure (de Grooth et al. 2015; Menne et al. 2016) was used to make six bi-layers NF PEMM. Polyethersulfone (PES) UF (MW = 20 kDa, Sterlitech Corporation) serving as support was soaked in deionized water (DI) overnight at 4°C before the coating and placed on a support device exposing the active side of the membrane for the LBL deposition. The support device is water-tight and does not permit leakage of the polyelectrolyte solution to the non-active side of the membrane. Each bi-layer is made up of one layer of polycation (Polydiallyldimethylammonium chloride (PDADMAC), MW = 400 – 500 kDa, Sigma Aldrich) and one layer of polyanion (Poly(styrenesulfonate) (PSS), MW = 1000 kDa, Sigma Aldrich) (figure S1).

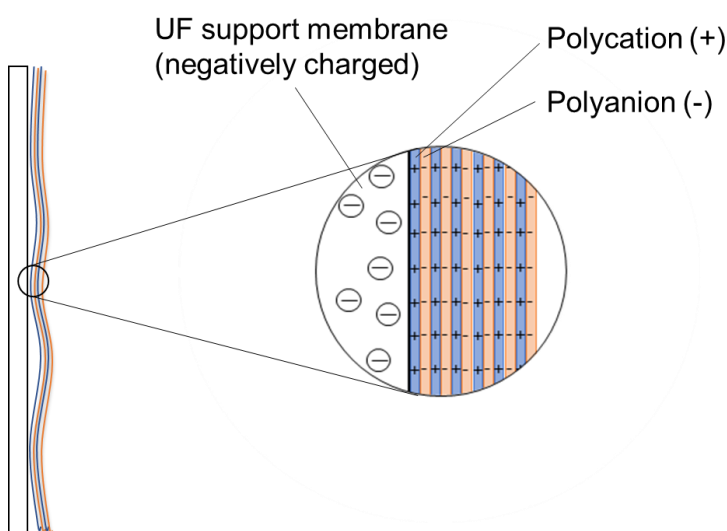


Figure S1: Schematic diagram of negatively charged UF coated with six polyelectrolyte bilayers.

The polyelectrolytes (PSS and PDADMAC) concentration was 1g/L in 0.5M NaCl (Merck) solution. Because PES is negatively charged, the first layer was a polycation (PDADMAC),

while the terminating layer was a polyanion (PSS) to encourage rejection of negatively charged ions ( $SO_4^{2-}$ ,  $PO_4^{3-}$ ). The polycation (PDADMAC) was first deposited on the PES surface, then rinsed before depositing polyanion (PSS) (figure S2). The duration for each deposition was 20 minutes, while the rinsing was 10 minutes; rinsing water is changed every 3 minutes. More details on the coating procedure are given in table S1. The process (figure S2) is repeated to the desired number of bi-layers. The membrane was stored in DI at 4°C until used.

Table S1: Details of the layer-by-layer coating procedure.

Polyelectrolyte Concentration	1 g/L
Ionic Strength	0.5 M NaCl
Polyelectrolyte adsorption time	20 min
Rinsing time (DI water)	10 min
Number of layers	6

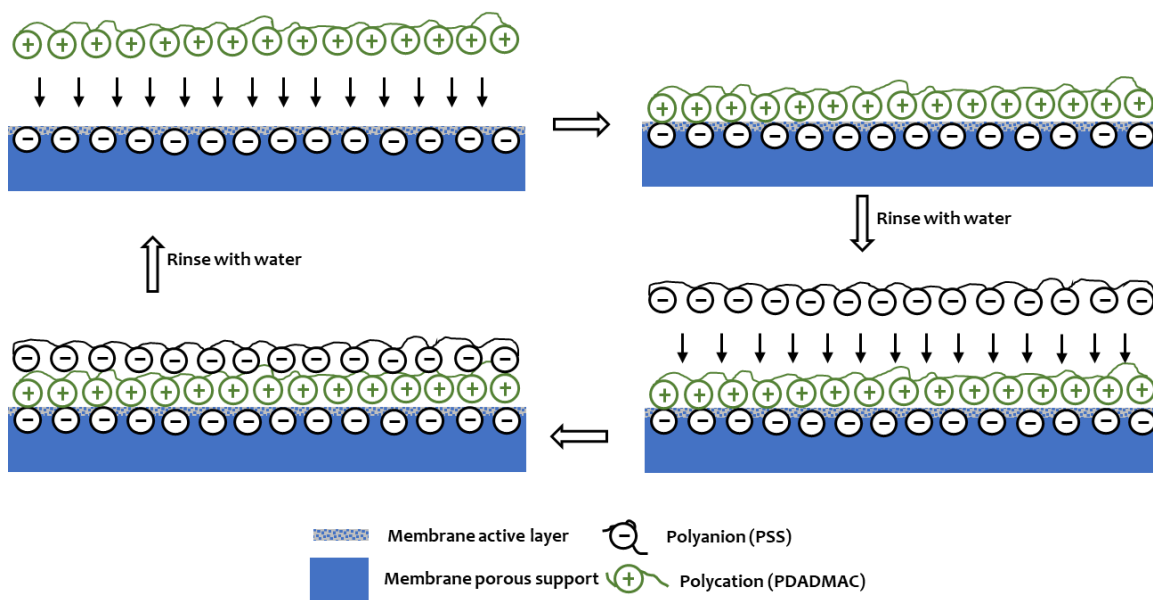


Figure S2: Polyelectrolyte multilayer membrane coating procedure

Pure water permeability (PWP) (deionized (DI) water, conductivity < 2  $\mu$ S/cm) and rejection measurements of selected solutes ((NaCl, Merck), magnesium sulfate ( $MgSO_4 \cdot 7H_2O$ , Merck) and a sodium phosphate buffer at pH = 7 ( $Na_2HPO_4$ , AnalaR, BDH Laboratory Supplies;  $NaH_2PO_4$ : Aldrich)) were used to characterize the coated membranes. Table S2 gives the results of the membrane PWP and solutes rejections for all coated membranes and after cleaning (done after each scaling experiment). The membrane was cleaned with 0.01M nitric acid (70%  $HNO_3$ ,

BioLab Ltd.). PWP and solute rejections were measured with permissible deviations of  $\pm 25\%$  and  $\pm 15\%$  for PWP and rejection, respectively, for reuse in the scaling experiments.

Table S2: Properties of NF-PEMMs used in the experiments

Membrane	PWP [LMH/bar]	Rejection			
		NaCl (0.1 M)	MgSO <sub>4</sub> (0.02 M)	Phosphate Buffer (0.1 M, pH = 7)	
1	Pristine	9.9	41.5	81.5	69.9
	After 1 <sup>st</sup> cleaning	8.6	41.7	81.2	-
2)*	Pristine	8.8	42.0	77.8	69.5
	After 1 <sup>st</sup> cleaning	8.2	41.7	85.3	-
3	Pristine	11.2	43.3	83.0	72.8
	After 1 <sup>st</sup> cleaning	9.5	41.6	89.6	-
	After 2 <sup>nd</sup> cleaning	8.2	41.7	88.3	-
	After 3 <sup>rd</sup> cleaning	8.5	41.2	84.9	-
4	After 4 <sup>th</sup> cleaning	8.5	41.6	86.1	-
	Pristine	11.5	42.3	69.6	61.2
	After 1 <sup>st</sup> cleaning	9.6	41.8	80.1	-

Table S3: Synthetic wastewater effluent chemical composition

Element	Ions	Concentration (mM)
Magnesium	Mg <sup>2+</sup>	1.15
Sulphate	SO <sub>4</sub> <sup>2-</sup>	1.15
Potassium	K <sup>+</sup>	0.6
Chloride	Cl <sup>-</sup>	14
Sodium	Na <sup>+</sup>	8.7
Dissolved inorganic carbon	DIC	5

Table S4: We used 1 M stock solutions of scaling salts for CaCO<sub>3</sub> and CaP fouling experiments; concentrations for each scaling component added is shown below. For CaCO<sub>3</sub> scaling, a combination of CaCl<sub>2</sub> and NaHCO<sub>3</sub> was added to the feed solution, while CaCl<sub>2</sub> and Na<sub>2</sub>HPO<sub>4</sub> were used for CaP scaling. For the low supersaturation experiment, salt additions were reduced to three for both salts while the respective mole addition remained the same.

Scalant	Salt 1		Salt 2	
CaCO <sub>3</sub>	CaCl <sub>2</sub>		NaHCO <sub>3</sub>	
Addition	[mmol/L]	[g/L]	[mmol/L]	[g/L]
1	8	1.18	8	0.67
all	56	8.26	56	4.07
Ca-P	CaCl <sub>2</sub>		Na <sub>2</sub> HPO <sub>4</sub>	
Addition	[mmol/L]	[g/L]	[mmol/L]	[g/L]
1	6	0.88	4	0.57
All	42	6.17	28	3.97

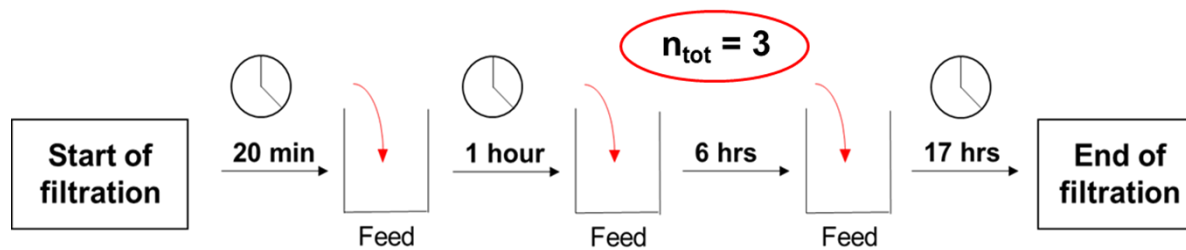


Figure S3: Procedure for the low supersaturation fouling investigation. The number of salt additions is reduced to three, with extended intervals between additions and the filtration time.

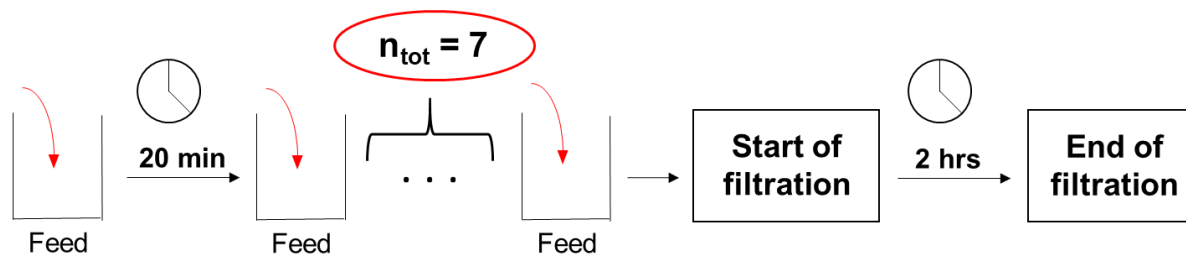


Figure S4: Procedure for the cake filtration-particulate fouling by CaCO<sub>3</sub> crystals. Concentration and the number of salt additions are the same as in section 3.1, and all salts are added to make a suspension before starting the filtration step.

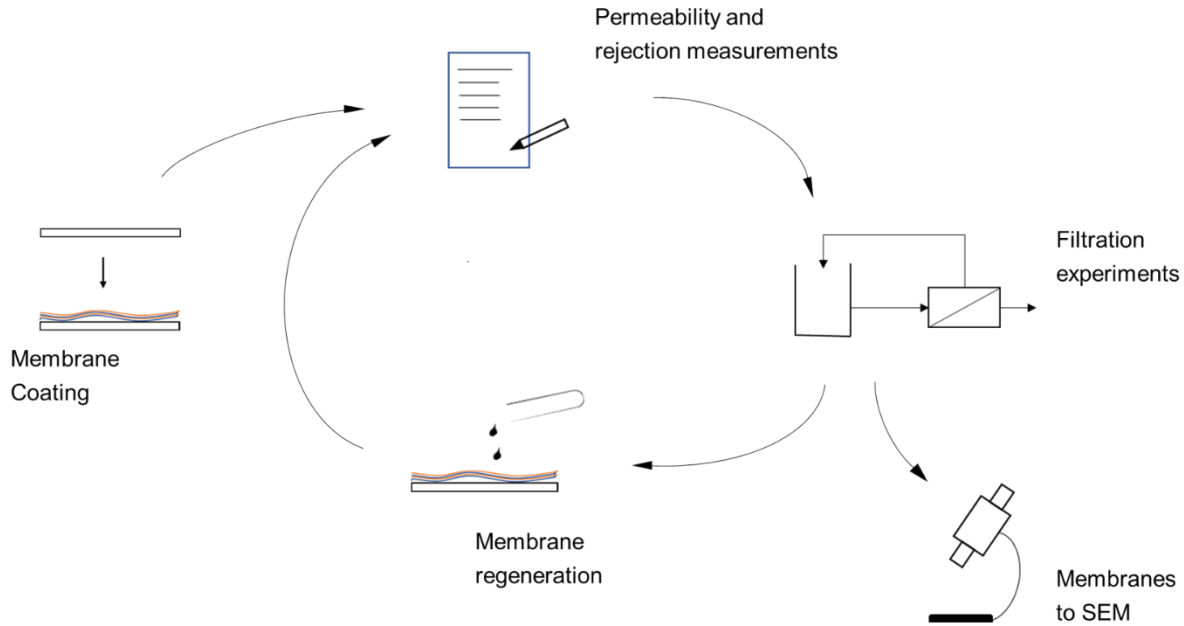


Figure S5: Experimental cycle: membrane coating with polyelectrolytes → membrane permeability and salt rejection tests → filtration experiments → (If required) membrane SEM analysis → membrane regeneration with nitric acid → membrane permeability and salt rejection tests → filtration experiments.

Table S5: Summary of the differences in the experiment modifications

Experiment Modifications	Scaling in high supersaturated effluent	Scaling in low supersaturated effluent	Cake layer hydraulic resistances
Time of addition	During filtration	During filtration	Before Filtration
Number of additions	7	3	7
Interval between additions	20 min	1, 3 and 6 h	20 min
Filtration time	4 h	24	4 H

## 2.0 Thermodynamic modelling using PHREEQC

PHREEQC is a general geochemical software for thermodynamic modelling, which applies to many hydrogeochemical environments (Parkhurst and Appelo 2013). It could simulate chemical reactions and transport processes in laboratory experiments, industrial processes, and natural/polluted waters (Parkhurst and Appelo 2013). We used Minteq.v4 database for the

model; added ACP, with its corresponding  $K_{sp}$  value (Combes and Rey 2010). PHREEQC was used to determine the mass-based precipitation potential of the  $\text{CaCO}_3$  added salts. The determined mass-based precipitation potential of  $\text{CaCO}_3$  was used to model CaP to have similar mass-based precipitation potential to enable comparison. The model parameters can be found in appendix A.

### 3.0 Scanning electron microscopy (SEM)

The scanning electron microscopy images (SEM) were acquired after filtration using ultrahigh-resolution JSM-7400F (FEG-SEM, JEOL SEM).

### 4.0 Membrane resistance calculations

In an equivalent circuit diagram, a membrane is represented by a parallel circuit of a capacitor  $C$  and a resistance  $G$  (Kavanagh et al. 2009; Długołęcki et al. 2010) (Figure S6 a). In the case of a frequency-independent system, there is no capacitor  $C$ , and the parallel circuit is simplified to a single ohmic resistance (Figure S6 b). For a complete and correct representation of the membrane-resolution system, two more resistances must be added to take account of the resistance of feed and permeate.

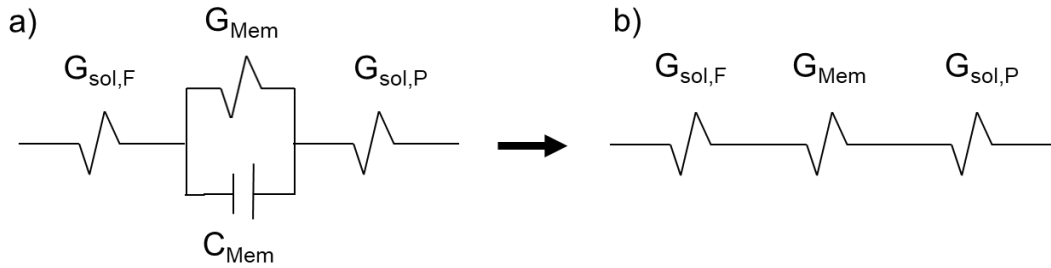


Figure S6: a) Original equivalent circuit diagram of the membrane - solution system. b) Simplified membrane-solution system for a frequency-independent system.

With this simplification, the impedance  $Z$  can be considered as series-connected resistances, according to the equation:

$$Z = R_{Mem} + R_{Sol,i} \quad (\text{Eq1})$$

Where  $R_{Mem}$  is the resistance of the membrane and  $R_{Sol,i}$  the resistances of the ambient solutions. Inserting the resistances of feed  $R_{Sol,F}$  and permeate  $R_{Sol,P}$ , the following equation applies:

$$Z = R_{Mem} + R_{Sol,F} + R_{Sol,P} \quad (\text{Eq2})$$

The equation is illustrated in Figure S7

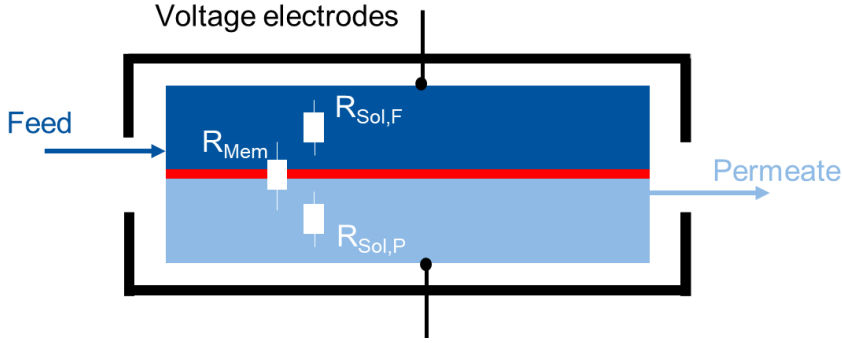


Figure S7: Schematic diagram of the longitudinal section of the membrane module. The measured impedance can be considered as series-connected resistances between the voltage electrodes.

The change of the membrane resistance with proceeding filtration time is especially insightful to detect fouling. An increasing resistance can refer to an additional layer on the membrane or an increased occurrence of ions (concentration polarization).

The continual electrical conductivity measurements of feed and permeate allowed calculating the resistance values for feed and permeate via the following equation.

$$\sigma = \kappa \cdot \frac{A}{l} \quad (\text{Eq3})$$

Equation (Eq3) gives the general equation for calculating a conductivity  $\sigma$  out of the specific conductivity  $\kappa$ , the cross-sectional area of the sample  $A$  and the sample length  $l$ . In the case of the membrane-solution system,  $A = 0.016 \text{ m}^2$  is the cross-sectional area of the membrane,  $l$  describes the distance between the voltage electrodes and was measured to  $l = 2 \text{ mm}$  (INPHAZE PTY LTD 2010). The values for  $\kappa$  were taken from the results of the electrical conductivity measurements. Thus, the absolute electrical conductivity values for feed and permeate could be calculated. Conductivity values can be transformed into resistances via the following equation:

$$R = \frac{1}{\sigma} \quad (\text{Eq4})$$

As a result, the quantities  $R_{\text{Sol},F}$  and  $R_{\text{Sol},P}$  are known. The EIS data gave the measurements of the impedance  $Z$ . After rearranging equation (), the membrane resistance could be calculated at several points in time:

$$R_{\text{Mem}} = Z - R_{\text{Sol},F} - R_{\text{Sol},P} \quad (\text{Eq5})$$

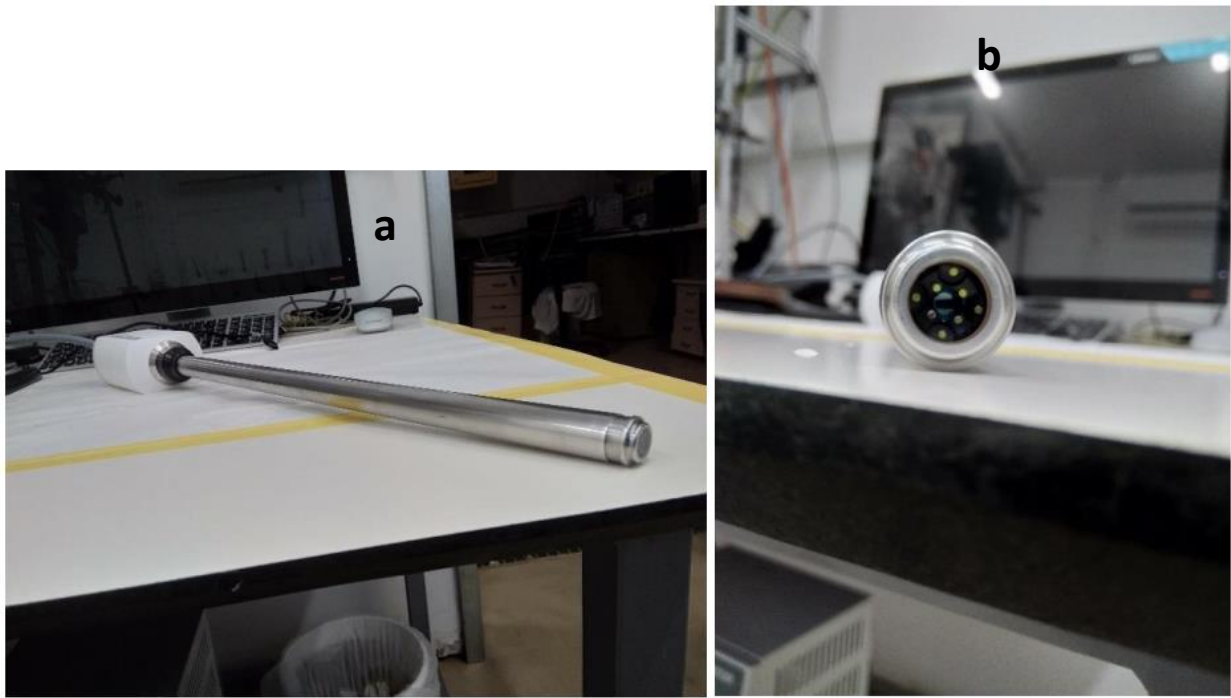


Figure S8: (a) particle view microscope; (b) camera window

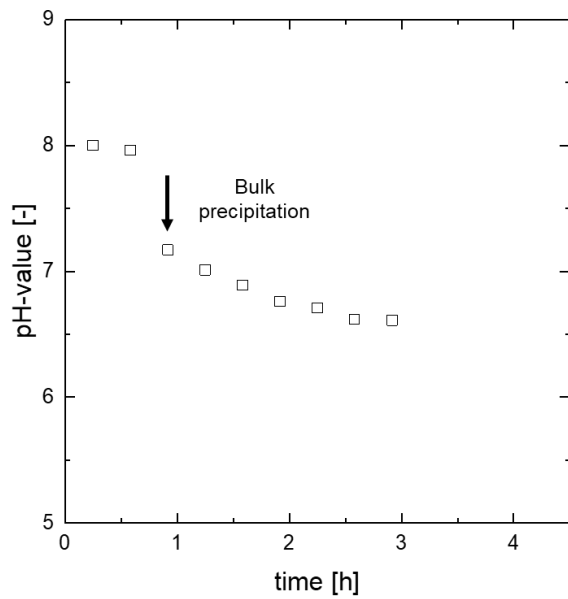


Figure S9: pH-value over time [h] during the  $\text{CaCO}_3$  high supersaturation scaling effluent nanofiltration. The pH-value drops with the third addition. At this point, bulk crystallization occurred.

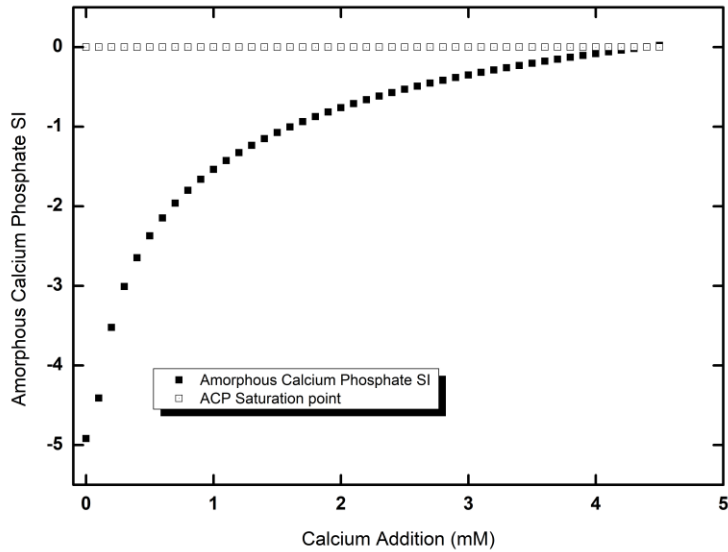


Figure S10: CaP (as amorphous calcium phosphate – ACP) saturation index (SI) evolution with calcium ion addition to a solution containing 2 mM of total P (added as a mixture of sodium dihydrogen phosphate and sodium hydrogen phosphate). SI (calculated using PHREEQC) rises with the addition of calcium and at SI ~0.00 lead to precipitation in the feed.

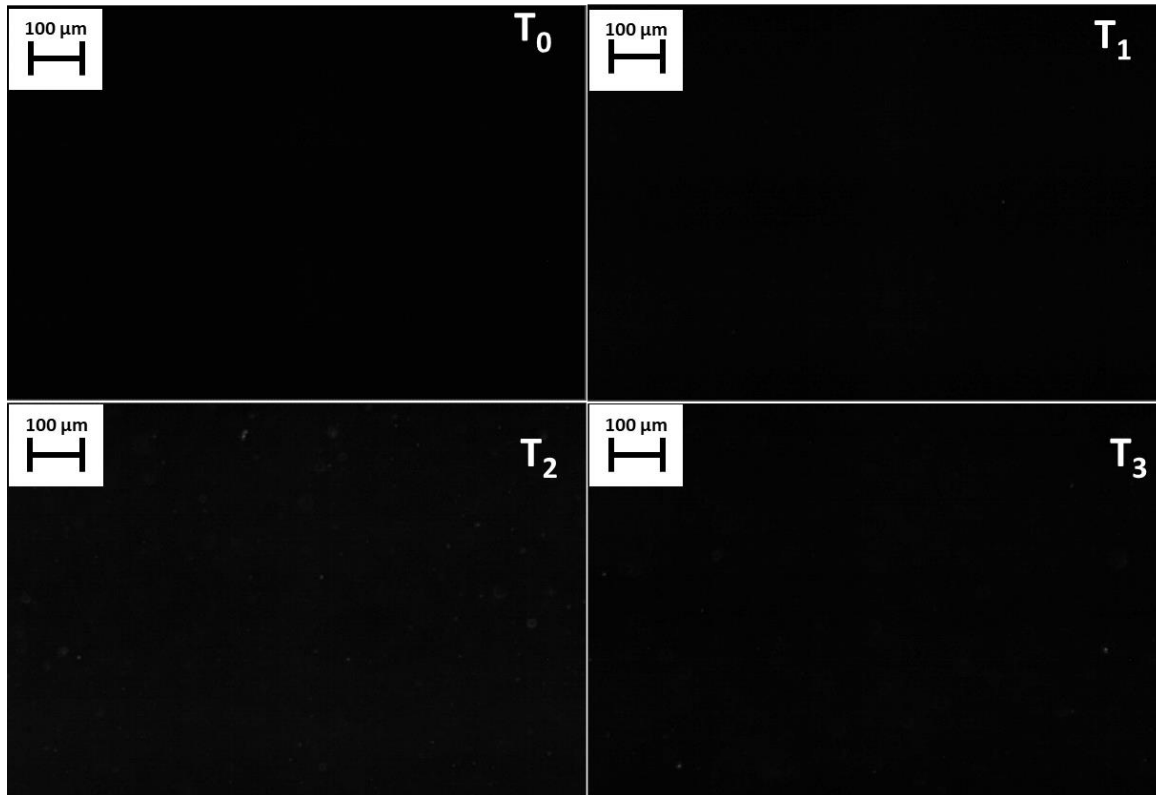


Figure S11: In-line real-time images of  $\text{CaCO}_3$  particle development over the filtration time [h] for nanofiltration of low supersaturated effluent. T indicates time, bulk precipitation was obvious from second and third salt additions. Although, there was a local action low-scale bulk

precipitation 30 minutes after the first addition of salts.  $T_0$  and  $T_1$  indicate blanks and represent time evolution between the addition of scaling salts and the start of precipitation.

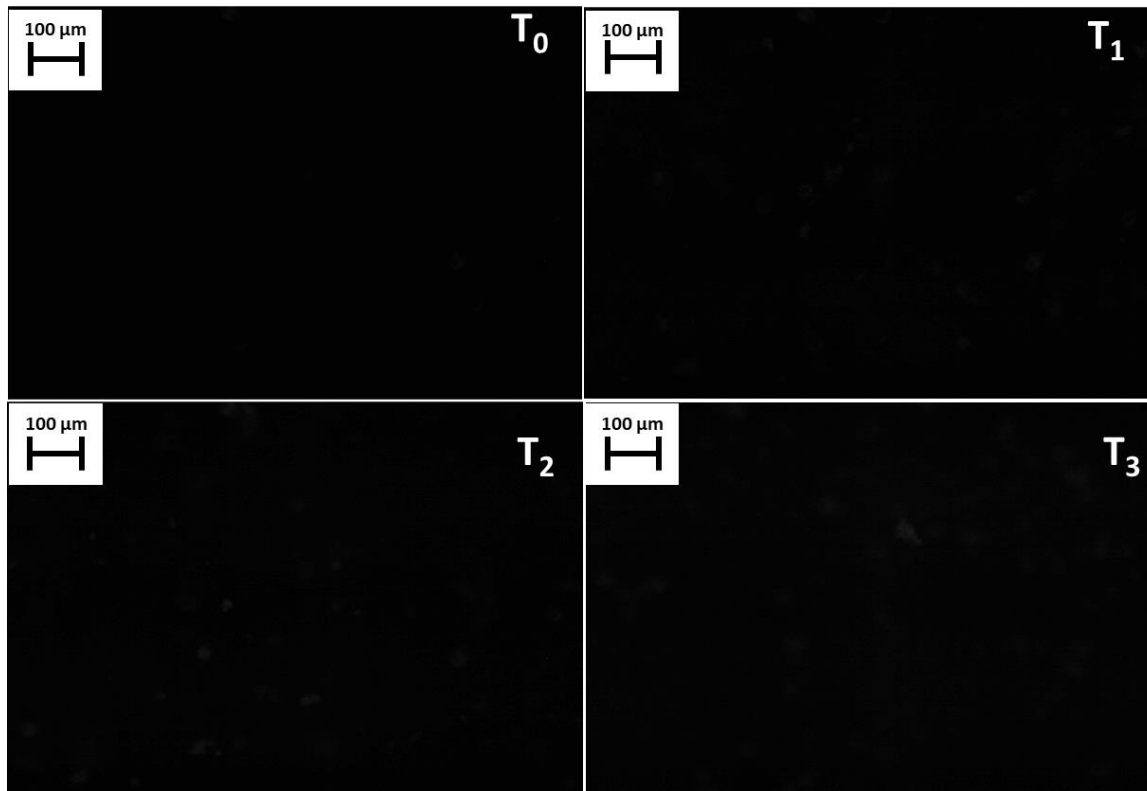


Figure S12: In-line real-time images of CaP particle development over the filtration time [h] for nanofiltration of low supersaturated effluent. T indicates time; bulk precipitation was evident from the first salt addition.  $T_0$  indicate blank while  $T_1$  represent time evolution for the addition of scaling salts and precipitation starts.

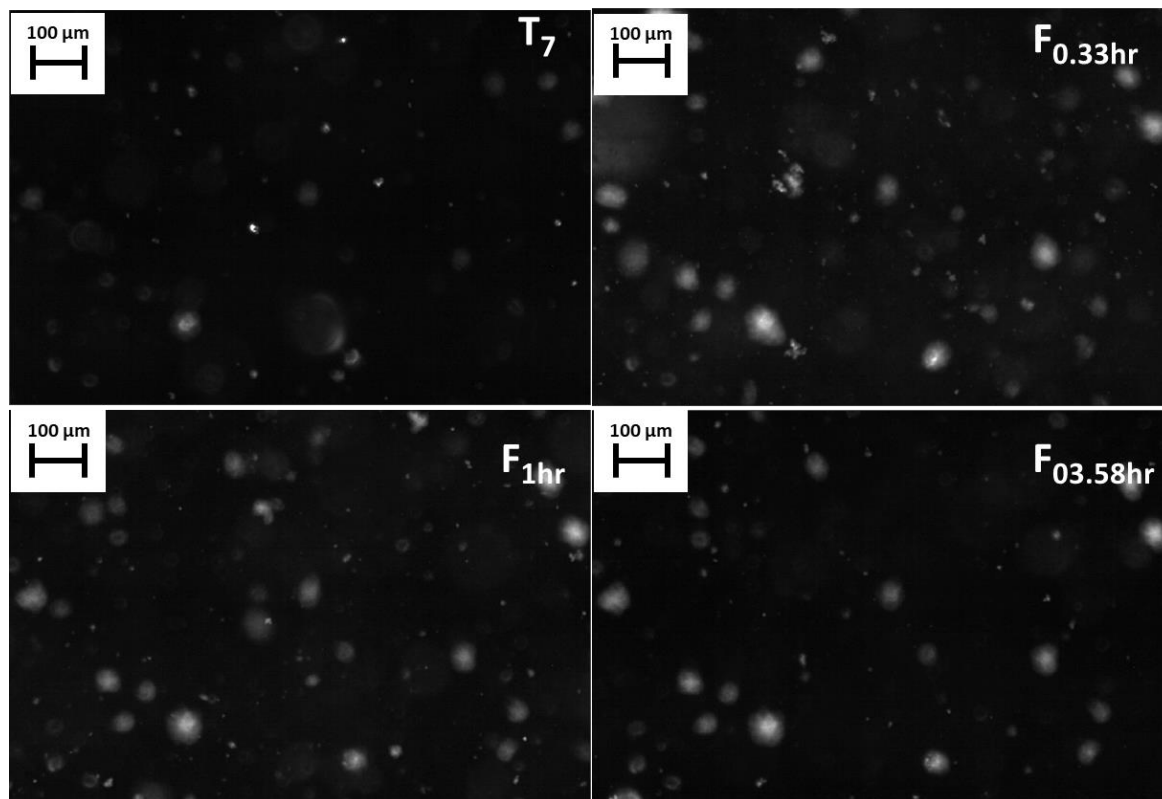


Figure S13: In-line real-time images of  $\text{CaCO}_3$  particle development over the filtration time [h] for nanofiltration of bulk crystallization-cake filtration. T indicates the time of salt addition, while F indicates filtration time.

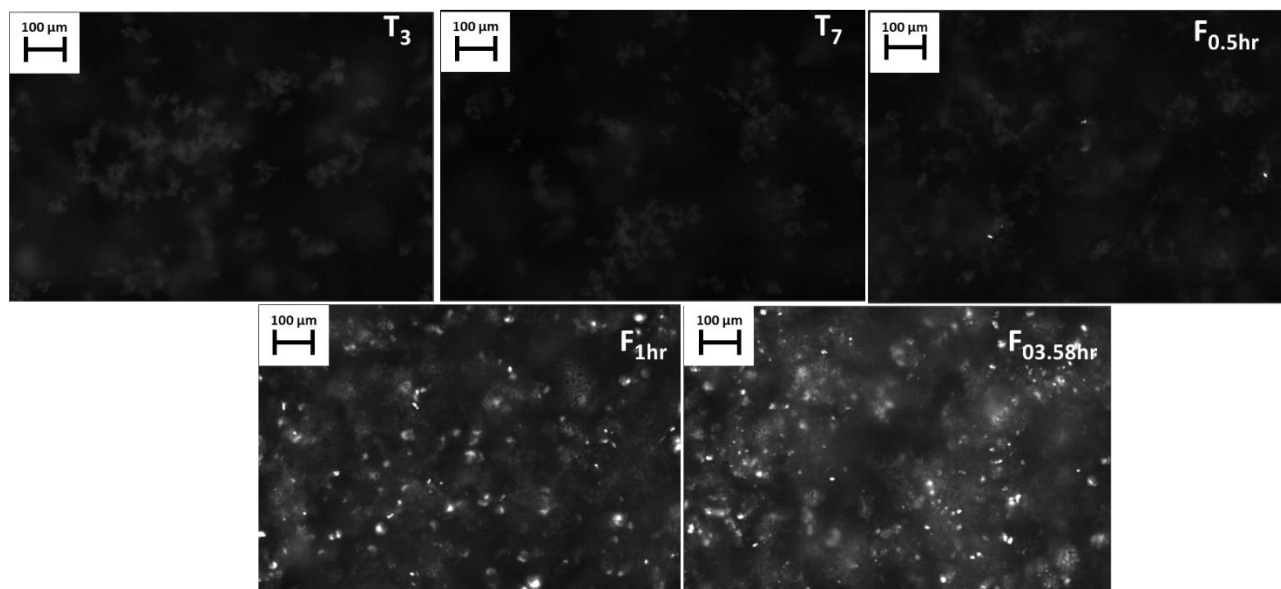


Figure S14: In-line real-time images of Ca-P particle development over the filtration time [h] for nanofiltration of bulk crystallization-cake filtration. T indicates image time of salt addition, while F indicates image at the time of filtration after all salts were added.

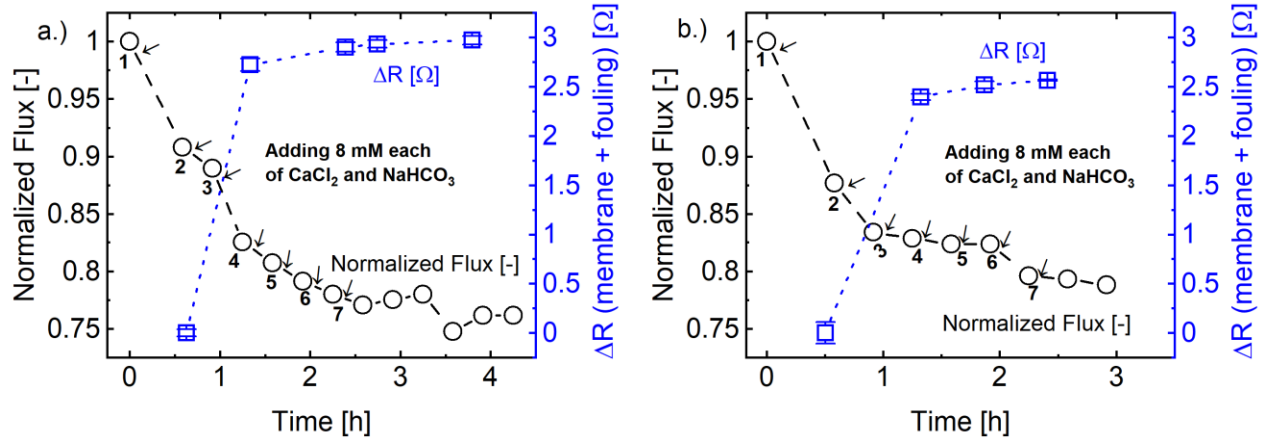


Figure S15: Repetition data recorded during nanofiltration of solutions highly supersaturated with calcium carbonate, (a) normalized flux-(O) (arrows everywhere in all figures indicate the addition of scaling components, immediately after permeability measurement. The first point is the permeability of the background solution without scaling salts, all permeability normalized to initial permeability) and membrane resistance-( $\square$ ) [ $\Omega$ ]. Electrical resistance data are presented as the average of (a. : N=6-10 and b. : N=7-10) multiple measurements where error bars are standard deviations. Similar 3-phase permeability decline (in two of the three experiments) and fouling resistance layer evolution shows experiments are reproducible.

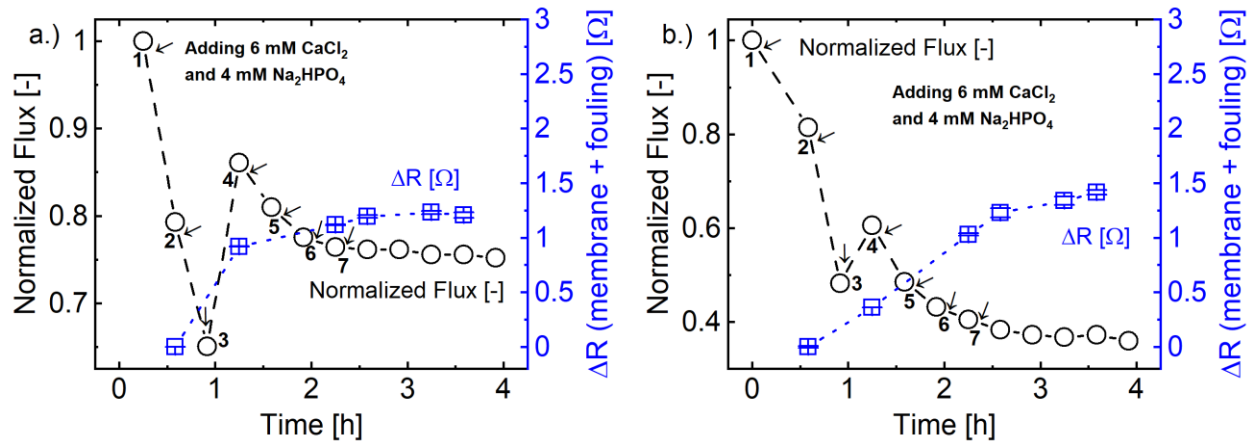


Figure S16: Repetition data recorded during nanofiltration of solutions highly supersaturated with calcium phosphate (a) permeability-(O) and membrane resistance-( $\square$ ) [ $\Omega$ ]. Electrical resistance data are presented as the average of (a. : N=10 and b. : N=3-10) multiple measurements where error bars are standard deviations. Similar 3-phase permeability decline and fouling layer resistance evolution shows experiments are reproducible.

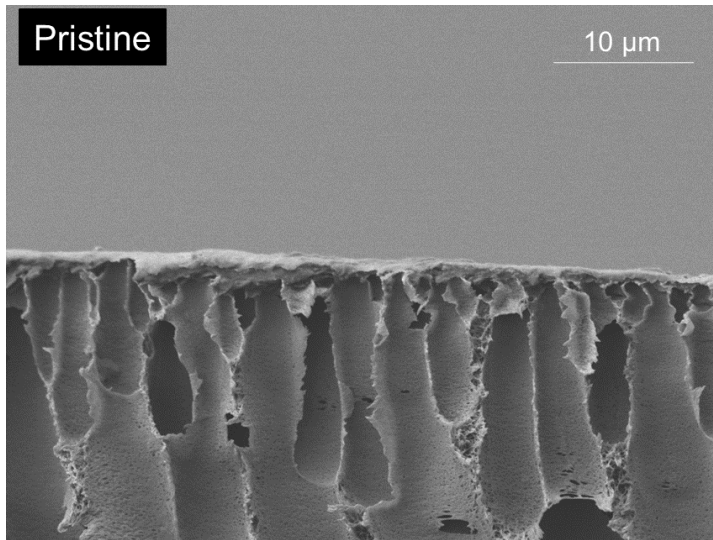


Figure S17: SEM image (cross-section) of pristine membrane over the filtration time [h] for simulated low supersaturation  $\text{CaCO}_3$  scaling

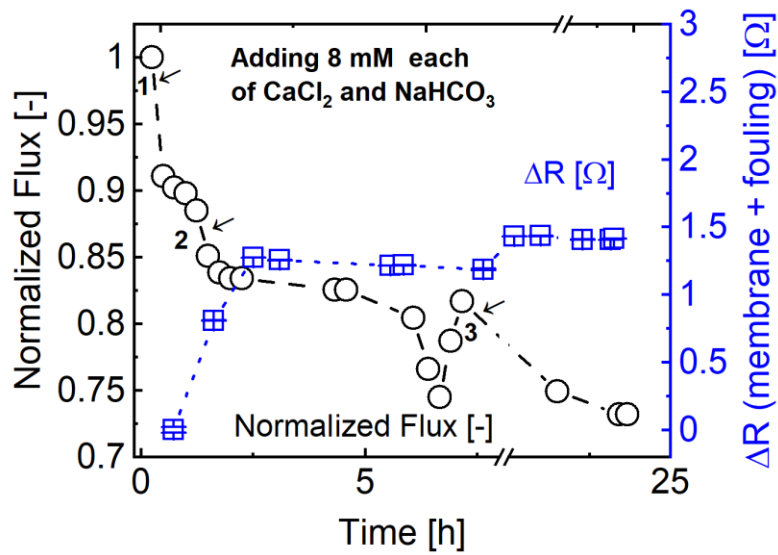


Figure S18: Extended normalized flux and fouling layer electrical resistance of  $\text{CaCO}_3$  scaling over filtration time [h] for nanofiltration of low supersaturated effluent. Electrical resistance data is presented as the average of (N=10) multiple measurements where error bars are standard deviations.

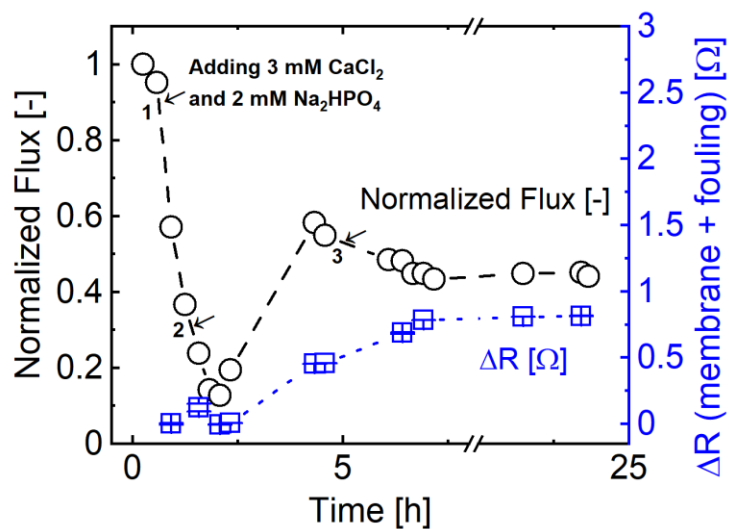


Figure S19: Extended normalized flux and fouling layer electrical resistance of CaP scaling over filtration time [h] for nanofiltration of low supersaturated effluent. Electrical resistance data is presented as the average of (N=10) multiple measurements where error bars are standard deviations.



Figure S20: In-line real-time image at T=3.25hr of  $\text{CaCO}_3$  particle development over the filtration time [h] for nanofiltration of high supersaturated effluent. Decreased RBI due to reduced particle concentration resulting from their contribution to cake layer build-up on the membrane surface.

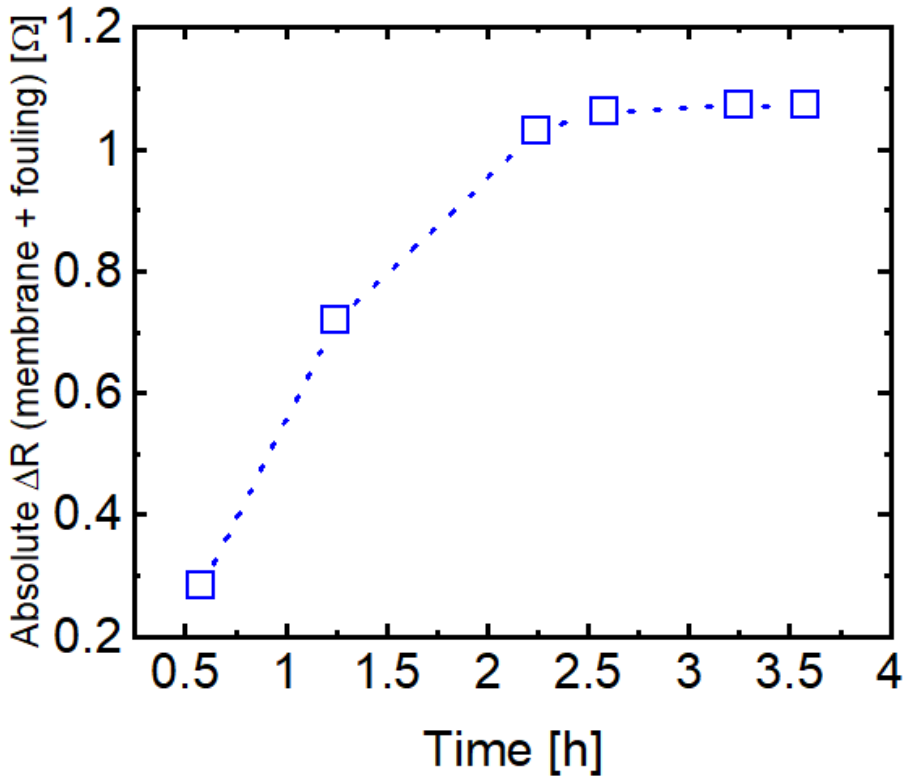


Figure S21: Absolute values of fouling layer electrical resistance over filtration time [h] during nanofiltration of CaP rapid increase supersaturation.

### 5.0 EIS INPHAZE™ crossflow module

The INPHAZE filtration module is a stainless-steel filtration cell operated in crossflow mode. It combines the EIS electrodes and an insulating layer with a membrane module, as shown in the cross-section/exploded view (Fig. S24). The module integrates four electrodes, thus using four

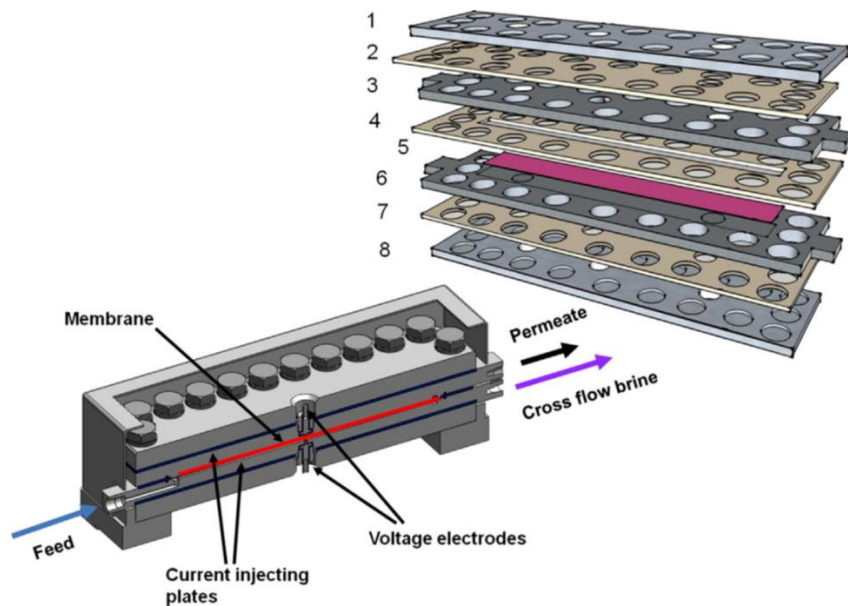


Figure S22: INPHAZE filtration module: cross-section (left) and explode view (right) (1 and 8: metal frame; 2 and 7: insulating separators; 3 and 6: metal plates with electrically insulated channels for voltage sensing electrodes; 4: gasket; 5: membrane) (Kavanagh et al. 2009; Ho et al. 2016)

terminal method to measure electrical impedance. Two plate electrodes are located close to the membrane and in contact with feed and permeate solutions (plates 3 and 6). These electrodes inject alternating current through the feed-membrane-permeate system. The potential is measured with two electrically insulated voltage sensing points on each side of the membrane. One voltage point is connected to the electrode in the top plate channel, while the other voltage point is connected to the bottom plate channel (1 and 8 respectively) (Coster et al. 1996; Antony et al. 2013). The interface between metal current injecting electrodes and their aqueous environments forms an electrical double layer that commonly gives rise to a separate frequency-dependent impedance. These strong impedances can be excluded from the measurement by segregating the two current-injecting electrodes from the voltage electrodes (Antony et al. 2013).

Additionally, potential measurement utilizes amplifiers of very high differential input impedance ( $10^{12} \Omega$ ). These amplifiers augment the low-level differential signals that develop across the system while dismissing unwanted signals of the electrode-solution interface. Hence, the current flowing through the interfaces between voltage electrodes and the feed/permeate solutions is negligible. Thus, the four-terminal method erases the effects of the frequency-dependent impedances arising from any electrode-solution interface (Coster et al. 1996).

Appendix:

A. PHREEQC calculations

PHASES

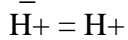
Struvite



log\_k -13.26

delta\_h 22.6 kJ

Fix\_H+



log\_k 0

MgSO4:7H2O



log\_k 10

Mg(OH)2



log\_k 10

Amor\_CalciumPhosphate



log\_k -25.46

delta\_h -440 kJ

Monetite



```

log_k -6.81
CaCl2:2H2O
CaCl2:2H2O = Ca+2 + 2Cl- + 2H2O
log_k 100
delta_h 30.6 kJ
NaHCO3
NaHCO3 = HCO3- + Na+
log_k 100
delta_h -950.8 kJ
Na2HPO4
Na2HPO4 = 2Na+ + HPO4-2
log_k 100
NaH2PO4
NaH2PO4 = Na+ + H2PO4-
log_k 100
SOLUTION 1
temp 25
pH 7
pe 4
redox pe
units mmol/l
density 1
Cl 28.3
K 0.6
Mg 1.15
Na 8.7
S 1.15
-water 1 # kg
REACTION 1 Addition of reactants
CaCl2:2H2O 3
Na2HPO4 2
1 millimoles in 1 steps
SAVE solution 1
END
USE solution 1
EQUILIBRIUM_PHASES 1
Amor_CalciumPhosphate 0 0
END
SOLUTION 2
temp 25
pH 8.5
pe 4
redox pe
units mmol/l
density 1
Cl 28.3

```

K 0.6  
Mg 1.15  
Na 8.7  
S 1.15  
-water 1 # kg  
REACTION 1 Addition of reactants  
CaCl2:2H2O 1  
NaHCO3 1  
8 millimoles in 1 steps  
SAVE solution 2  
END  
USE solution 2  
EQUILIBRIUM\_PHASES 2  
Calcite 0 0  
SOLUTION 3  
temp 25  
pH 7  
pe 4  
redox pe  
units mmol/kgw  
density 1  
-water 1 # kg

## Reference

- Antony A, Chilcott T, Coster H, Leslie G (2013) In situ structural and functional characterization of reverse osmosis membranes using electrical impedance spectroscopy. *J Memb Sci*. doi: 10.1016/j.memsci.2012.09.028
- Combes C, Rey C (2010) Amorphous calcium phosphates: Synthesis, properties and uses in biomaterials. *Acta Biomater* 6:3362–3378. doi: 10.1016/J.ACTBIO.2010.02.017
- Coster HGL, Chilcott TC, Coster ACF (1996) Impedance spectroscopy of interfaces, membranes and ultrastructures. In: *Bioelectrochemistry and Bioenergetics*
- de Grooth J, Haakmeester B, Wever C, et al (2015) Long term physical and chemical stability of polyelectrolyte multilayer membranes. *J Memb Sci* 489:153–159. doi: <https://doi.org/10.1016/j.memsci.2015.04.031>
- Długolecki P, Ogonowski P, Metz SJ, et al (2010) On the resistances of membrane, diffusion boundary layer and double layer in ion exchange membrane transport. *J Memb Sci*. doi:

10.1016/j.memsci.2009.11.069

Ho JS, Sim LN, Gu J, et al (2016) A threshold flux phenomenon for colloidal fouling in reverse osmosis characterized by transmembrane pressure and electrical impedance spectroscopy. *J Memb Sci* 500:55–65. doi: 10.1016/J.MEMSCI.2015.11.006

INPHAZE PTY LTD CPA (2010) Cross-Flow Chamber Assembly Instructions. In: Rev.C12. pp 10–13

Kavanagh JM, Hussain S, Chilcott TC, Coster HGL (2009) Fouling of reverse osmosis membranes using electrical impedance spectroscopy: Measurements and simulations. *Desalination*. doi: 10.1016/j.desal.2007.10.066

Menne D, Kamp J, Erik Wong J, Wessling M (2016) Precise tuning of salt retention of backwashable polyelectrolyte multilayer hollow fiber nanofiltration membranes. *J Memb Sci* 499:396–405. doi: 10.1016/j.memsci.2015.10.058

Parkhurst DL, Appelo CAJ (2013) Description of input and examples for PHREEQC version 3: a computer program for speciation, batch-reaction, one-dimensional transport, and inverse geochemical calculations. US Geological Survey